Water Reuse

IWA PUBLISHING

Water Reuse Vol 13 No 1, 68 doi: 10.2166/wrd.2023.071

Deep learning algorithms were used to generate photovoltaic renewable energy in saline water analysis via an oxidation process

Wongchai Anupong[a], Abolfazl Mehbodniya[b], Julian L. Webber[b], Ali Bostani[c], Gaurav Dhiman[d,e,f], Bharat Singh[g] and Murali Dharan A. R.[h,*]

[a] Independent Researcher (Thailand), Department of Agricultural Economy and Development, Faculty of Agriculture, Chiang Mai University, Chiang Mai 50200, Thailand
[b] Department of Electronics and Communication Engineering, Kuwait College of Science and Technology (KCST), Doha Area, 7th Ring Road, Doha Area, Kuwait
[c] College of Engineering and Applied Sciences, American University of Kuwait Salmiya, Salmiya, Kuwait
[d] Department of Electrical and Computer Engineering, Lebanese American University, Byblos, Lebanon
[e] Department of Computer Science and Engineering, University Centre for Research and Development, Chandigarh University, Gharuan, Mohali 140413, India
[f] Department of Project Management, Universidad Internacional Iberoamericana, Campeche, Mexico
[g] Mechanical Engineering, GLA University Mathura, Mathura, UP, India
[h] Debre Berhan University, Debre Berhan, Ethiopia
*Corresponding author. E-mail: mdharan75@dbu.edu.et

ABSTRACT

The amount of particles and organic matter in wash-waters and effluent from the processing of fruits and vegetables determines whether they need to be treated to fulfil regulatory standards for their intended use. This research proposes a novel technique in photovoltaic cell-based renewable energy in saline water analysis using the oxidation process and deep learning techniques. Here, the saline water oxidation is carried out based on photovoltaic cell-based renewable and saline water analysis is done using Markov fuzzy-based *Q*-radial function neural networks (MFQRFNN). The plan is entirely web-oriented to enable better control and effective monitoring of water consumption. This monitoring makes use of a communication system that collects data in the form of irregularly spaced time series. Experimental analysis has been carried out based on water salinity data in terms of accuracy, precision, recall, specificity, computational cost, and kappa coefficient.

Key words: deep learning, oxidation process, photovoltaic cell, renewable energy, saline water analysis

HIGHLIGHTS

- This research proposes a novel technique in photovoltaic cell-based renewable energy in saline water analysis using the oxidation process and deep learning techniques.
- Forecasting energy demand is an essential component of PV that aids in the planning of power generation as well as energy trading with a commercial grid.
- Deep learning-based models hold great promise for forecasting consumer demands and RES energy generation.

1. INTRODUCTION

Analysing water use is important because it helps building managers and operators adopt better usage planning strategies (Alshehri *et al.* 2021). Forecasting is crucial for effective consumption management and ongoing monitoring. Additionally, efficient detection and prevention of water leaks and waste in distribution networks and installations depend on accurate forecasting of use. There have been several approaches investigated to anticipate water demand and usage in close to real-time. Thereafter, more or less successful ways include statistical techniques, filtering and signal processing methods, fuzzy logic, intelligent strategies, and combinations of many models (Elsheikh *et al.* 2022). More recently, cutting-edge models like machine learning (ML) have demonstrated greater performance than traditional models. Deep neural networks (DNN) in particular have become effective forecasting techniques. Regardless of the approach, the forecasting performance's robustness is primarily influenced by context and environmental data, redundant measurement systems, and the short, medium, and long-term planning choices that need to be made. When no data are available to support the usage of a single water metre, projecting water demand remains a significant research challenge (Said *et al.* 2022). To forecast and

prepare for the management of water quality, a variety of physical or mathematical models have been created, but they are complicated, time-consuming, and data-intensive. Users in poor nations that have limited data or background information find these models difficult to employ. On the basis of both linear and nonlinear correlations between input and output variables, statistical models of water quality have been constructed. Nevertheless, in situations with multivariate nonlinear connections, these models frequently fall short of accurately capturing the complexity of these events (Maddah *et al.* 2020). Numerous water quality indices have nonlinear, stochastic, and lagged correlations, making it difficult to develop a mathematical model to forecast events under these conditions using conventional methods (Parida *et al.* 2021). Recent years have seen research on artificial intelligence (AI) algorithms for water quality modelling. In order to create models that best capture these interactions, these algorithms investigate obscure and intricate correlations between input and output variables. The data required for AI models can often be obtained from remote sensing platforms, and they have a number of advantages over conventional physical and statistical models, including the following: they are less sensitive to missing data than conventional approaches, their structures are flexible, nonlinear, and robust, and they can handle massive amounts of data and data of various scales (Trappey *et al.* 2019).

Contribution of this research is as follows:

1. To propose novel technique in photovoltaic cell-based renewable energy in saline water analysis using oxidation process and deep learning techniques.
2. The saline water oxidation is carried out based on photovoltaic cell-based renewable and saline water analysis is carried out using Markov fuzzy-based *Q*-radial function neural networks (MFQRFNN).

Organisation of this article is as follows: section 2 discusses existing techniques in renewable energy in saline water analysis, section 3 explains novel saline water analysis based on oxidation process and deep learning techniques, performance analysis with discussion is given in section 4 and the conclusion of this research with a future scope is given in section 5.

2. RELATED WORKS

A number of ML methods can be a potential solution to deal with multiple linear regression (MLR) methods' limitations. Artificial neural networks (ANNs) are a promising alternative to traditional mathematical models for solving nonlinear issues in science and engineering because of their straightforward construction (Wang *et al.* 2022). According to work (Coşgun *et al.* 2021), ML algorithms and efficient use of field data are helpful in modelling water quality factors which may then be taken into consideration for treatment unit sizing. To further enhance the quality and sustainability of the wastewater treatment process, various optimisation techniques have been developed (Salem *et al.* 2022a). This method is incredibly efficient and simple to use for issues with highly linked input parameters. However, they are unable to produce an explicit equation between the input variables and the output variable(s) which is crucial for engineering problems with real-world applications (Jamei *et al.* 2021). The group method of data handling (GMDH) approach is a trustworthy and self-organising neural network sub-model among the numerous intelligence techniques. The detection of plant diseases, the modulus of a pressure metre, the temperature of the soil, the dispersion coefficients in water pipes, and the small strain shear modulus of grouted sands are just a few nonlinear problems where this method is successfully used (Hu & You 2022). Aslam *et al.* (2021) employed a method for evaluating air enteric viruses discharged from wastewater for irrigation and performed a quantitative microbial risk analysis (QMRA). They discovered that although it requires more computing time, the outcome may help to establish safe water recycling laws. In contrast to conventional methods, Sharma *et al.* (2022) proposed using ANN for disinfection, which may improve predictions of the inactivation of microorganisms over time as well as other physiochemical water parameters, such as temperature and pH (Potential of Hydrogen) value. Bu *et al.* (2021) develops the use of AI for a range of classifications as well as prediction difficulties. It also explains how hybrid AI is used to extract, classify, forecast, and model characteristics utilising a variety of algorithms and optimisation techniques (Tang *et al.* 2020). In a study (Sohani *et al.* 2022), ANNs were used to model the nonlinear operation of biotechnology. Along with these methods, a variety of ML methods have also been used to solve the issue, such as multi-layer perceptron (MLP) (Wang *et al.* 2021), support vector regression (SVR) (Nazari *et al.* 2022), and more recently random forest (RF) in Dave *et al.* (2020). In the scheme of groundwater prediction, the application of Extreme Gradient Boosting (XGB) is uncommon and is seen in only a few studies such as Pombo *et al.* (2022). To estimate ΔTWS, Salem *et al.* (2022b) carefully chose 11 hydrological factors, including total precipitation as well as snow cover. Regarding the idea of utilising prior pixels to anticipate present pixels, the literature does not go into enough detail. SVMs and RF were compared by Meng *et al.* (2021) for predicting current

grid-based rainfall up to 3 h in advance, with input being previous radar-derived rainfall. According to Shalaby *et al.* (2022), entire water vapour photos were predicted using ANNs every 30 min using data from two prior photographs.

3. SYSTEM MODEL

This section discusses novel techniques in photovoltaic cell-based renewable energy in saline water analysis using the oxidation process and deep learning techniques. The saline water oxidation is carried out using photovoltaic cell-based renewable and saline water analysis is carried out using Markov fuzzy based *Q*-radial function neural networks (MFQRFNN).

3.1. Photovoltaic cell-based renewable energy in saline water analysis using oxidation process

A solar panel, a boost converter, and MPPT controller made up the photovoltaic method, as represented in Figure 1.

An electronic component known as a photovoltaic (PV) cell produces electricity when exposed to sunshine. The solar cell can be used separately or alongside other solar cells in a photovoltaic panel. PV cell models come in a variety of forms, each with varying degrees of complexity and accuracy. The electrical circuit shown in Figure 2 which is equivalent to a photovoltaic cell can be used to represent them.

Equations (1) and (2) represent the current of the PV cell as follows:

$$I = I_{\text{ph}} - I_{\text{o}}\left\{\exp\left[\frac{q}{nN_s kT}(V + IR_{\text{s}})\right] - 1\right\} - \frac{V + IR_{\text{s}}}{R_{\text{sh}}} \tag{1}$$

$$V_{\text{T}} = \frac{N_5 nkT}{q} \tag{2}$$

V_{T} is the thermal voltage, N_{s} is the cells connected in series; n is the diode ideality constant; q is the charge of electron; k is the Boltzmann constant; T is the temperature of $p - n$ junction; I_{ph} is the photo-current; I_0 is the reverse saturation currents of diode.

To collect maximum power generated and incurred load, a static converter (DC/DC power converter) is employed as an adapter between PV generators and load. In order to provide constant maximum power efficiency, the boost converter is managed by an MPPT (maximum power point tracking) controller. This programme uses an iterative approach based on a method to obtain maximum power delivered by PV, as represented in Figure 3.

A single PV system operating in islanded mode exhibits a number of drawbacks, such as reduced dependability and a constrained capacity for energy production. The connectivity of various microgrids can address this problem by changing the power flows to and from the connected microgrid modules in response to power imbalances. The setup taken into consideration in this paper uses a STATCOM/ESS module to regulate the microgrid's active and reactive power. Through tie-lines,

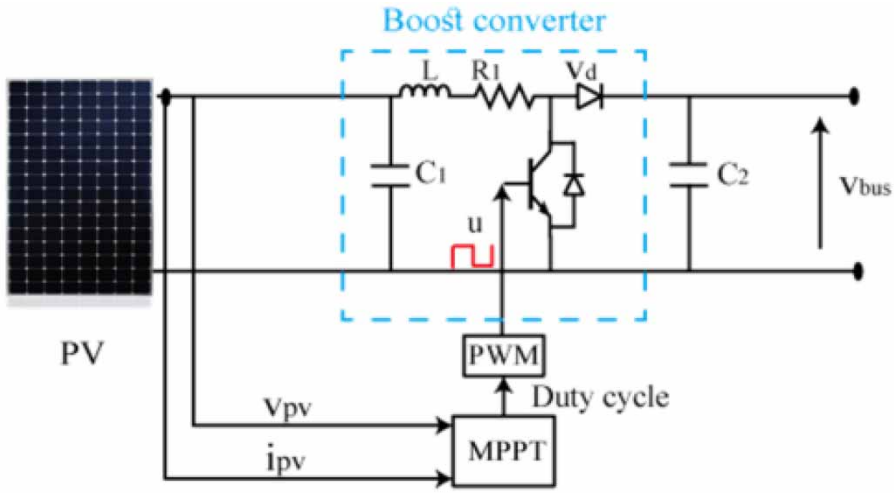

Figure 1 | Photovoltaic system.

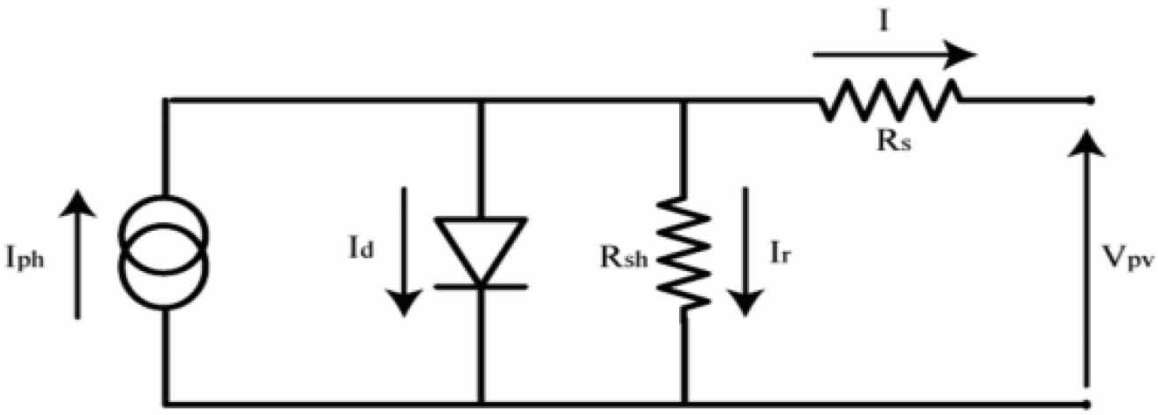

Figure 2 | Equivalent electrical diagram of a photovoltaic cell.

inverters and ESSs are utilised to exchange power among interconnected microgrids. Based on frequency measurements, the power flow between the interconnected microgrids is managed. Direct electric current was connected to each aluminium electrode in the series. An AC/DC current exchanger supplied the electric current. Sodium chloride was utilised to generate synthetic wastewater with certain salt content. The chemical oxygen demand (COD) and total organic carbon (TOC) concentrations as a result were 3,500 and 2,000 mg/L, respectively. 1 N NaOH and HCl solutions were employed to change the pH. All chemical experiments were carried out in accordance with the prescribed procedures. Responses of COD and TOC removal efficiencies by Equation (3) were used to evaluate the process' performance:

$$\text{COD or TOC removal efficiency } (\%) = \left(\frac{c_i - c}{c_i}\right) \times 100 \tag{3}$$

c_i and c are the starting as well as ultimate concentrations of COD or TOC (mg/L), respectively. In order to maximise the factors affecting the removal of COD as well as TOC from saline solutions, RSM was utilised. pH, reaction time, salt content, and voltage at three coded levels were three independent variables that were looked at (Table 1). Preliminary screening

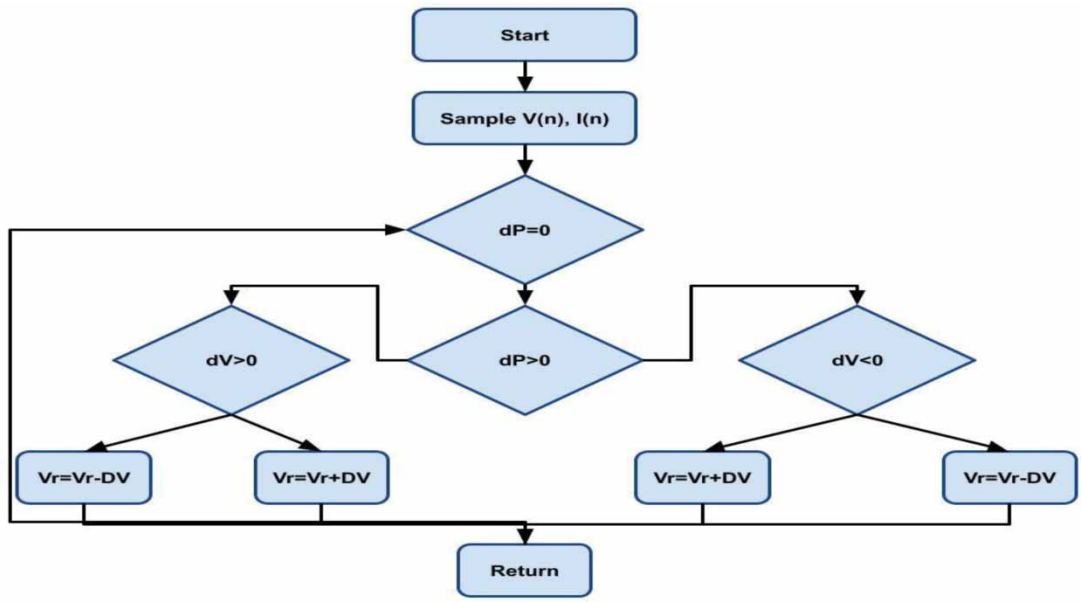

Figure 3 | Flowchart of MPPT method.

Table 1 | Comparative analysis between proposed and existing technique based on various saline water analysis

Salt water analysis	Techniques	Accuracy	Precision	Recall	Specificity	Computational cost	Kappa coefficient
$S = 35$–140 g/L	GMDH	82	70	65	58	45	32
	SVM	84	72	68	62	48	33
	PRE_SWA_DL	86	74	72	63	51	39
$T_{cond} = 20$–30 °C	GMDH	85	73	66	64	53	35
	SVM	88	76	69	66	55	38
	PRE_SWA_DL	91	80	74	71	56	42
$T_{evap} = 60$–80 °C	GMDH	93	82	69	65	54	39
	SVM	94	84	72	69	56	43
	PRE_SWA_DL	96	86	76	73	58	45

studies as well as literature reviews provided the variable ranges. The experimental design used in this study was a two-level full factorial design with additional central as well as star points. According to Equation (4), total number of experiments (N) can be computed:

$$N = N_a + N_0 + N_c \tag{4}$$

where N_0 is the number of replications in the central point for evaluating net error (five replications), N_a is the number of two-level experiments, and N_c is number of star points (24). So, a total of 29 experiments were created. The software Design Expert 7 was used to do statistical design of trials as well as data analysis. The following equation can be used to represent the second-order method equation for the prediction of the ideal conditions: In the experiments, every variable was optimised. Analysis of Variance (ANOVA) was used to analyse data as well as identify interactions between independent variables of process as well as responses. The experiments were carried out at random to avoid systemic error. The performance of independent variables is determined by coefficients of second-order method, which interpret the degree of removal of researched parameters. Multiple regressions were used to assess the research data. Fischer test was used to control the statistical significance, while determination coefficients were used to control the quality of method fitting (F-test).

3.2. Markov fuzzy-based *Q*-radial function neural networks (MFQRFNN) based saline water analysis

Assume that X_t is a realisation of the MRF represented by X_t. The label field can be calculated for any feature extraction issue by maximising the posterior probability distribution given by the following equations:

$$\hat{x}_t = \arg\max_{x_t} P(X_t = x_t | Y_t = y_t) \tag{5}$$

$$\hat{x}_t = \arg\max_{x_t} \frac{P(Y_t = y_t | X_t = x_t) P(X_t = x_t)}{P(Y_t = y_t)} \tag{6}$$

where the estimated labels are indicated by $\hat{x}_t$. Since $P(Y_t = y_t)$ is a constant prior probability, (6) simplifies to Equation (7):

$$\hat{x}_t = \arg\max_{x_t} P(Y_t = y_t | X_t = x_t, \theta) P(X_t = x_t, \theta) \tag{7}$$

where the clique potential function of $xt's$ parameter vector is called θ. The MAP estimate is shown here as x_t. $P(X_t = x_t)$, the prior probability, and $P(Y_t = y_t | X_t = x_t, \theta)$ the likelihood function are the two components of Equation (7). It is possible to write the prior probability $P(X_t = x_t)$ as the following equation:

$$P(X_t = x_t, \theta) = \frac{1}{z} e^{\frac{-U(x_t)}{T}} = \frac{1}{z} e^{\frac{-\{\sum_{c \in C} V_c(x_t)\}}{T}} \tag{8}$$

where $U(X_t)$ is the energy function and z is the partition function written as $z = \sum_{x_t} e^{-U(x_t)/T}$ (a function of clique potentials). The clique potential function is represented by $V_c(x_t)$ in the spatial domain. It can be defined by equations in terms of the bonding parameter of the MRF model Equations (9) and (10):

$$V_c(x_t) = \begin{cases} +\alpha \text{ if } x_{st} = x_{qt} \\ -\alpha \text{ if } x_{st} \neq x_{qt} \end{cases} \tag{9}$$

$$V_{sc}(x_{st}, x_{qt}) = \begin{cases} +\alpha \text{ if } x_{st} \neq x_{qt} \text{ and } (s, t), (q, t) \in S \\ -\alpha \text{ if } x_{st} = x_{qt} \text{ and } (s, t), (q, t) \in S. \end{cases} \tag{10}$$

where q is a nearby site of s and is the bonding parameter for the MRF model α. It is understood that if X_t is an MRF, it meets the spatial direction of the Markovianity property by the following equation:

$$P(X_{st} = x_{st} | X_{qt} = x_{qt}, \forall q \epsilon S, s \neq q) = P(X_{st} = x_{st} | X_{qt} = x_{qt}, (q, t) \epsilon \eta_{st}) \tag{11}$$

The temporal evolution of these quantities is given by the following equations:

$$\rho_i^{S,g}(t+1) = \rho_i^{S,g}(t)(1 - \Pi_i^g(t)), \tag{12}$$

$$\rho_i^{E_I g}(t+1) = \rho_i^{S_g g}(t)\Pi_i^g(t) + (1 - \eta^g)\rho_i^{E_G}(t), \tag{13}$$

$$\rho_i^{A,g}(t+1) = \eta^g \rho_i^{E,g}(t) + (1 - \alpha^g)\rho_i^{A,g}(t), \tag{14}$$

$$\rho_i^{I_i^g}(t+1) = \alpha^g \rho_i^{A,g}(t) + (1 - \mu^g)\rho_i^{d_i^d}(t), \tag{15}$$

$$\rho_i^{H,g}(t+1) = \mu^9 \gamma^g \rho_t^{t,g}(t) + \omega^\theta (1 - \psi^g)\rho_i^{H,g}(t) + (1 - \omega^g)(1 - \chi^g)\rho_t^{H,g}(t). \tag{16}$$

$$\rho_i^{D,g}(t+1) = \omega^{g^s \psi^s \rho_i^{H,g}}(t) + \rho_i^{D,g}(t), \tag{17}$$

$$\rho_i^{R,g}(t+1) = \mu^g (1 - \gamma^g)\rho_i^{t_i^s g}(t) + (1 - \omega^g)x^g \rho_i^{H,g}(t) + \rho_i^{R,g}(t). \tag{18}$$

$$V_{\text{teec}}(x_{st}, x_{er}) = \begin{cases} +\gamma \text{ if } x_{st} \neq x_{er}, (s, t), (e, r) \epsilon S, t \neq r, \text{ and } r \in \{(t-1), (t-2)\} \\ -\gamma \text{ if } x_{st} = x_{er}, (s, t), (e, r) \in S, t \neq r, \text{ and } r \in \{(t-1), (t-2)\}. \end{cases} \tag{19}$$

Probability is given by the following equations:

$$\Pi_i^g(t) = (1 - p^g)P_i^g(t) + p^p \sum_{j=1}^{N} R_{ij}^g P_j^g(t), \tag{20}$$

$$m_k = \frac{\sum_{i=1}^{k+1} \psi_i}{l}, k = 1, \ldots, q - 1 + 1. \tag{21}$$

$$E(|\eta_i \cap A|) = \int_A k_1^{(1)}(x)\mathrm{d}x \tag{22}$$

$$E(|\gamma_1 \cap A_1||\gamma_t \cap A_2) = \int_{A_1}\int_{A_2} k_t^{\infty D}(x_1, x_2)\mathrm{d}x_2\mathrm{d}x_1 + \int_{A_5 \cap A_2} k_i^{(1)}(x)\mathrm{d}x \tag{23}$$

$$E(|\gamma_t \cap A_1||\gamma_{t+\Delta t} \cap A_2|) = \int_{A_1}\int_{A_2} k_{t,\Delta}(x_1, x_2)\mathrm{d}x_2\mathrm{d}x_1 + \int_{A_5 \cap A_2} k_i^{(1)}(x)\mathrm{d}x \tag{24}$$

A type-2 fuzzy set $\tilde{M}_{ij}^Q$ is represented as the following equation

$$\tilde{M}_{ij}^Q = \{(p_{ij}, \mu_{M_{ij}^Q}), \mu_{\tilde{M}_{ij}^Q}(p_{ij}, \mu_{M_{ij}^Q}) \quad \begin{matrix} \forall p_{ij} \in I, \\ \forall \mu_{M_{ij}^Q} \in J_{p_{ij}} \subseteq [0, 1]\} \end{matrix} \tag{25}$$

where p_{ij} is the pixel at I_j in centre of a window of the dimensions $(2Q+1)$ $(2Q+1)$ in the input picture I, M. Type-2 membership function Q_{ij}. The mean of the k-middle is determined as Equation (26) for a n element set $X_{ij}^{Q} = x_1, x_2, x_3,\ldots, x_n$ retrieved from a window of size $(2Q+1)$ where, X_{ij}^{Q} $(2Q+1)$ Equation (26):

$$m_k(X_{ij}^{Q}) = \begin{cases} \dfrac{1}{2k-1}\displaystyle\sum_{i=q-k+1}^{q+k-1} x_i & \text{for odd } n \\ & (n = 2q-1) \\ \dfrac{1}{2k}\displaystyle\sum_{i=q-k+1}^{q+k} x_i & \text{for even } n \\ & (n = 2q) \end{cases} \tag{26}$$

Each element of the type-1 fuzzy set, $X_{ij}^{Q} = x_1, x_2, x_3,\ldots, x_n$, in a window of size $(2Q+1)$ $(2Q+1)$ has an associated GMF defined as the following equation:

$$\mu_{M_{ij}}^{(Q,k)}(x_n) = e^{-(x_n - v_{ij}^{(Q)}}} \tag{27}$$

Then, q distinct means are produced as equation using the k-middle mean Equation (28):

$$\sigma_{ij}^{Q} = m_h(\Omega_{ij}^{Q}) \tag{28}$$

Equations (29) and (30) are used to calculate the standard deviation for k-middle means in a window:

$$\Omega_{ij}^{Q} = |x_n - v_{\text{avg}}|, \forall x_n \in X_{ij}^{Q} \tag{29}$$

$$v_{\text{avg}} = \frac{1}{q}\sum_{k=1}^{q} v_{ij}^{(Q,k)} \tag{30}$$

The second sub step involves obtaining a matrix Δ_{ij} utilising the q membership values for every window's dominant convolved feature. Matrix Δ_{ij} can be written as Equation (31) in mathematics:

$$\Delta_{ij} = \begin{bmatrix} \mu_{M_{ij}}^{(Q,1)}(x_1) & \mu_{M_{ij}}^{(Q,1)}(x_2) & \ldots & \mu_{M_{ij}}^{(Q,1)}(x_n) \\ \mu_{M_{ij}}^{(Q,2)}(x_1) & \mu_{M_{ij}}^{(Q,2)}(x_2) & \ldots & \mu_{M_{ij}}^{(Q,2)}(x_n) \\ \ldots & \ldots & \ldots & \ldots \\ \mu_{M_{ij}}^{(Q,q)}(x_1) & \mu_{M_{ij}}^{(Q,q)}(x_2) & \ldots & \mu_{M_{ij}}^{(Q,q)}(x_n) \end{bmatrix} \tag{31}$$

Equation (32) gives the energy of a combined configuration of its visible variables (v) and hidden variables (h):

$$E(\mathbf{v}, \mathbf{h}; \theta) = -\sum_{ij} \mathbf{W}_{ij}\mathbf{v}_{\boldsymbol{h}}\mathbf{h}_j - \sum_{i} \mathbf{b}_i\mathbf{v}_i - \sum_{j} \mathbf{a}_j\mathbf{h}_j \tag{32}$$

Equation (33) may be used to determine the joint probability of v and h which represents the parameter $\{\mathbf{W}, \mathbf{a}, \mathbf{b}\}$:

$$P_\theta(\mathbf{v}, \mathbf{h}) = \frac{1}{Z(\theta)}\exp(-E(\mathbf{v}, \mathbf{h}; \theta)) \tag{33}$$

The partition function in this context is denoted by $Z(\theta)$. The previous equation can be written as the following equation:

$$P_\theta(\mathbf{v}, \mathbf{h}) = \frac{1}{Z(\theta)}\exp\left(\sum_{i=1}^{D}\sum_{j=1}^{F} \mathbf{w}_{ij}\mathbf{v}_i\mathbf{h}_j + \sum_{i=1}^{D} \mathbf{v}_i\mathbf{b}_i + \sum_{j=1}^{F} \mathbf{h}_j\mathbf{a}_j\right) \tag{34}$$

The goal is to increase the likelihood function $P(v)$. Edge distribution of $P(v, h)$ can be used to determine $P(v)$ using the following equation:

$$P_\theta(\mathbf{v}) = \frac{1}{Z(\theta)} \sum_{\mathbf{w}} \exp[\mathbf{v}^T \mathbf{w}\mathbf{h} + \mathbf{a}^T \mathbf{h} + \mathbf{b}^T \mathbf{v}] \tag{35}$$

The RBM parameters are obtained by maximising $P(v)$. We maximise $\log(P(v)) = L(\theta)$ to maximise $P(v)$. First, stochastic gradient descent is used to maximise $L(\theta)$. $L(\theta)'$ derivative for W is then calculated using the following equation:

$$\frac{\partial L(\theta)}{\partial \mathbf{W}_{ij}} = \frac{1}{N} \sum_{m=1}^{N} \frac{\partial}{\partial W_{ij}} \log\left(\sum_{\mathbf{h}} \exp[\mathbf{v}^{(\omega)T} \mathbf{W}\mathbf{h} + \mathbf{a}^T \mathbf{h} + \mathbf{b}^T \mathbf{v}^{(0)}] \right) - \frac{\partial}{\partial W_{ij}} \log Z(\theta) \tag{36}$$

The average values of v_i and h_j from all of the datasets are obtained. First half of the formula is simple to calculate. Second half of the equation, which includes all $2|v| + |h|$ combinations of v and h, is equivalent to Equation (37) but it is challenging to solve because of the computational complexity:

$$\sum_{v,h} v_i h_j P_\theta(v, h) \tag{37}$$

To generate samples that fulfil distribution, a Markov chain with a stationary distribution $P(v)$ is first built. Gradient is then approximated using Monte Carlo simulations by the following equations:

$$\Delta \mathbf{a}_i = v_i^{(0)} - v_j^{(k)} \tag{38}$$

$$\Delta \mathbf{b}_i = P(\mathbf{h}_j = 1|\mathbf{v}^{(0)}) - P(\mathbf{h}_j = 1|\mathbf{v}^{(k)}). \tag{39}$$

$$.\Delta \mathbf{W}_{ij} = P(\mathbf{h}_j = 1|\mathbf{v}^{(0)})\mathbf{v}_i^{(0)} - P(\mathbf{h}_j = 1|\mathbf{v}^{(k)})\mathbf{v}_i^{(k)} \tag{40}$$

When $v(k)$ I is the sample that satisfies distribution $P(v)$ discovered through sampling and $v(0)$ I is the sample value. Finally, Equations (41)–(43) provide the parameter update equation:

$$a_i = a_i + \Delta a_i \tag{41}$$

$$\mathbf{b}_j = b_j + \Delta b_j \tag{42}$$

$$\mathbf{W}_{ij} = \mathbf{W}_{ij} + \Delta \mathbf{W}_{ij} \tag{43}$$

In Equations (44) and (45), the probability distribution is given:

$$P(V, h^{\mathrm{a}}, h^{\mathrm{A}}) = \frac{1}{\mathbf{Z}(\theta)} \exp - E(V, h^{h^{\mathrm{an}}, h^{\mathrm{A}}; \theta)} \tag{44}$$

$$P(V, h^{(0)}, h^{(1)}) = -V^{\tau} W^{(0)} h^{(0)} - V^{\tau} W^{(t)} h^{(2)} + b \tag{45}$$

Its construction includes both an encoder and a decoder. Simple matrix multiplication is used for both the encoder and decoder. As a normalising function, gradient function for the encoder is employed. After adjusting weight and biases, autoencoder's network is trained using the following equations:

$$h^{w} = a(b^{(n)} + V^T w^{(n)}) \tag{46}$$

$$h^{(m)} = a(b_i^{(n)} + h^{(n-1)T} W^{(n)}) \text{ where, } n = 1, 2, 3 \ldots, \tag{47}$$

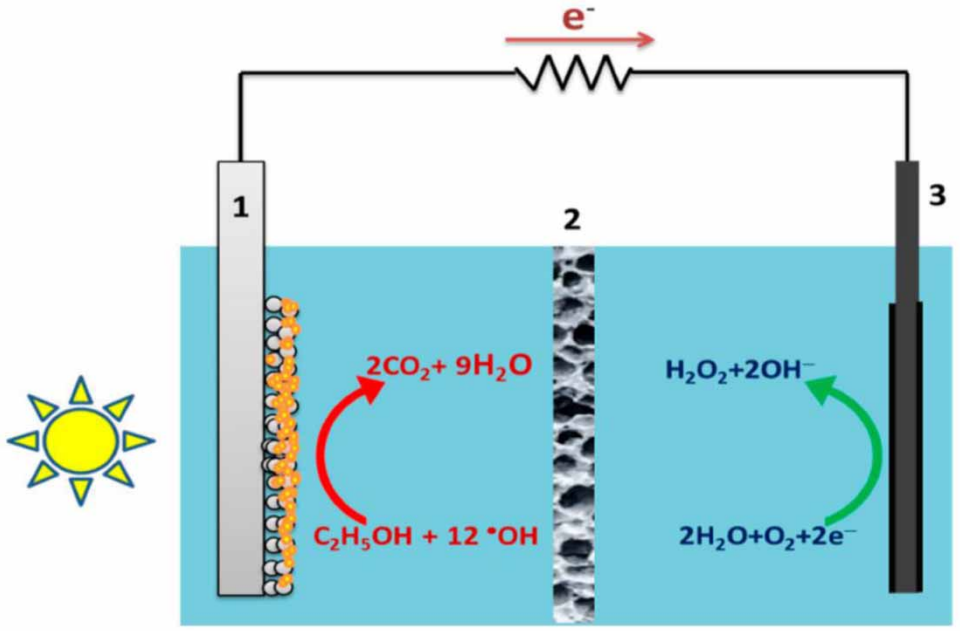

Figure 4 | Water oxidation in the PEC system.

However, because oxidation potential depends on photoinduced holes in the valence band edge of photoanode. Post Enumeration Checks (PEC) for the development of H_2O_2 (hydrogen peroxide) is yet only partially achieved. Following this revelation, the team concentrated on the WOR's production to better understand the mechanism. They found that when HCO_3 (bicarbonate) was present, substantial amounts of H_2O_2 instead of O_2 (dioxygen) generated, surprisingly accomplishing simultaneous H_2O_2 and H_2 (Hydrogen) production through PEC water splitting (Figure 4).

4. PERFORMANCE ANALYSIS

The experiment was carried out using a computer with the following technological specs: Intel Core i5 7200U, 8 GB of RAM, a 1 TB hard drive, and NVIDIA GTX 760MX graphics. Additionally, Python 3.5 environments were used to mimic implementation of the suggested approach. We conducted a statistical study by evaluating predicted performance to establish the findings of the suggested strategy.

4.1. Dataset description

The feed flow rate ($F = 400$–600 L/h), permeate flux (Pflux (L/h $\cdot$ m^2)), condenser inlet temperature ($T_{cond} = 20$–30 °C), evaporator inlet temperature ($T_{evap} = 60$–80 °C), and feed salt concentration ($S = 35$–140 g/L) made up the datasets. The principal output was permeate flux. To train NN, data have also been separated into three categories: training, validation, and testing. The training division is typically utilised to get model specifications. While testing division confirms its performance, the validation division checks precision of continuous training to prevent overfitting.

Table 1 gives a comparative analysis between the proposed and existing technique based on salt water analysis. Here the salt water analysis has been carried out based on salinity and temperature analysis of water like $S = 35$–140 g/L, $T_{cond} = 20$–30 °C, $T_{evap} = 60$–80 °C. Parameters analysed are in terms of accuracy, precision, recall, specificity, Computational cost, and Kappa coefficient.

Figure 5(a)–5(f) gives a comparative analysis between the proposed and existing technique for $S = 35$–140 g/L based on water salinity. Here the proposed technique attained accuracy of 86%, precision of 74%, recall of 72%, specificity of 63%, Computational cost of 51%, and Kappa coefficient of 39%, the existing GMDH (Group Method of Data Handling) attained accuracy of 82%, precision of 70%, recall of 65%, specificity of 58%, computational cost of 45%, Kappa coefficient of 32%, and the support vector machine (SVM) attained accuracy of 84%, precision of 72%, recall of 68%, specificity of 62%, computational cost of 48%, and Kappa coefficient of 33%.

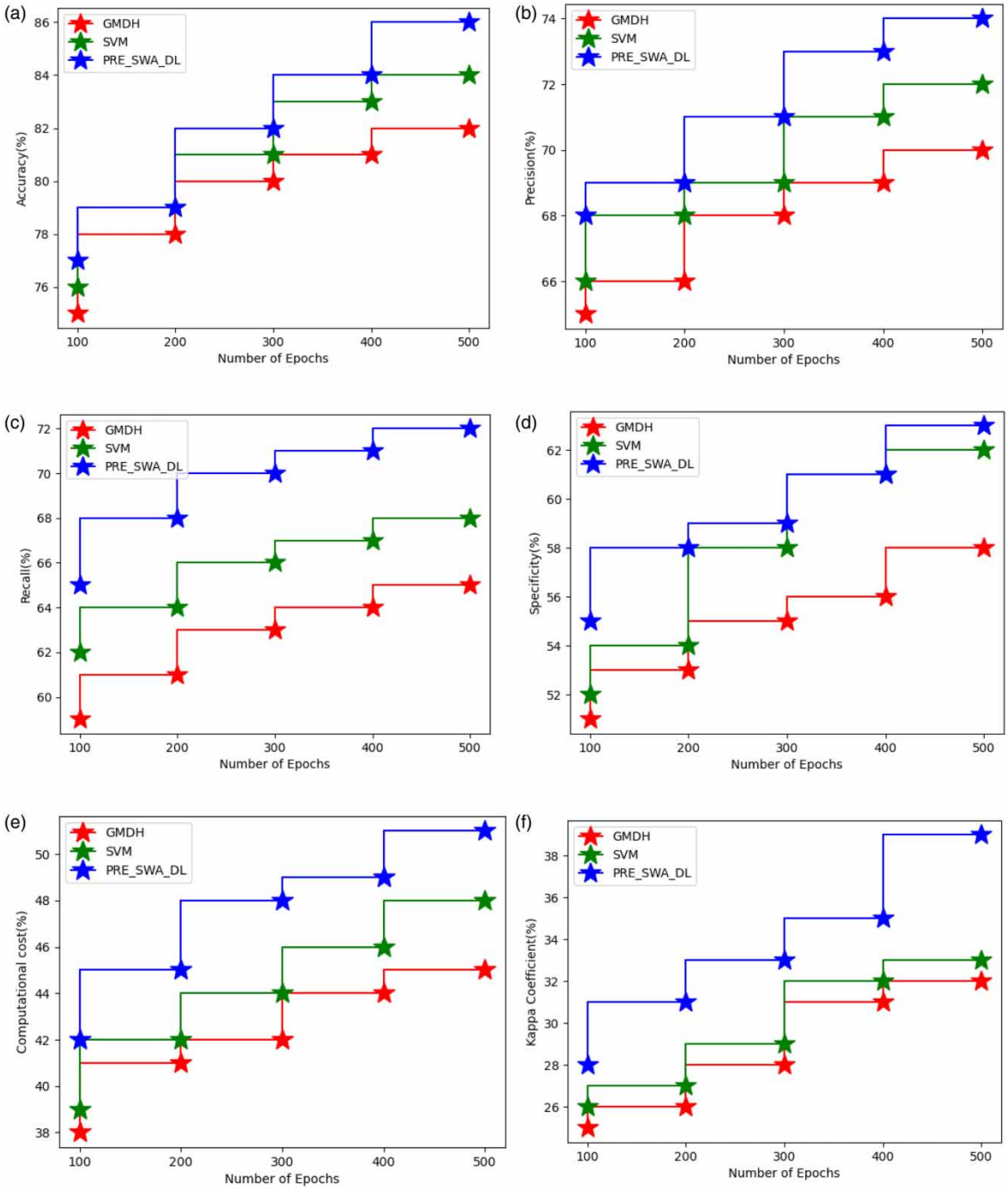

Figure 5 | Comparative analysis between proposed and existing technique for $S = 35$–140 g/L based on water salinity in terms of (a) Accuracy, (b) Precision, (c) Recall, (d) Specificity, (e) Computational cost, (f) Kappa coefficient.

Figure 6(a)–6(f) gives comparative analysis between the proposed and existing technique for $T_{cond} = 20$–30 °C based on water salinity. Proposed technique attained accuracy of 91%, precision of 80%, recall of 74%, specificity of 71%, computational cost of 56%, and Kappa coefficient of 42%. The existing GMDH attained accuracy of 85%, precision of 73%, recall of 66%, specificity of 64%, computational cost of 53%, and Kappa coefficient of 35%. SVM attained accuracy of 88%, precision of 76%, recall of 69%, specificity of 66%, computational cost of 55%, and Kappa coefficient of 38%.

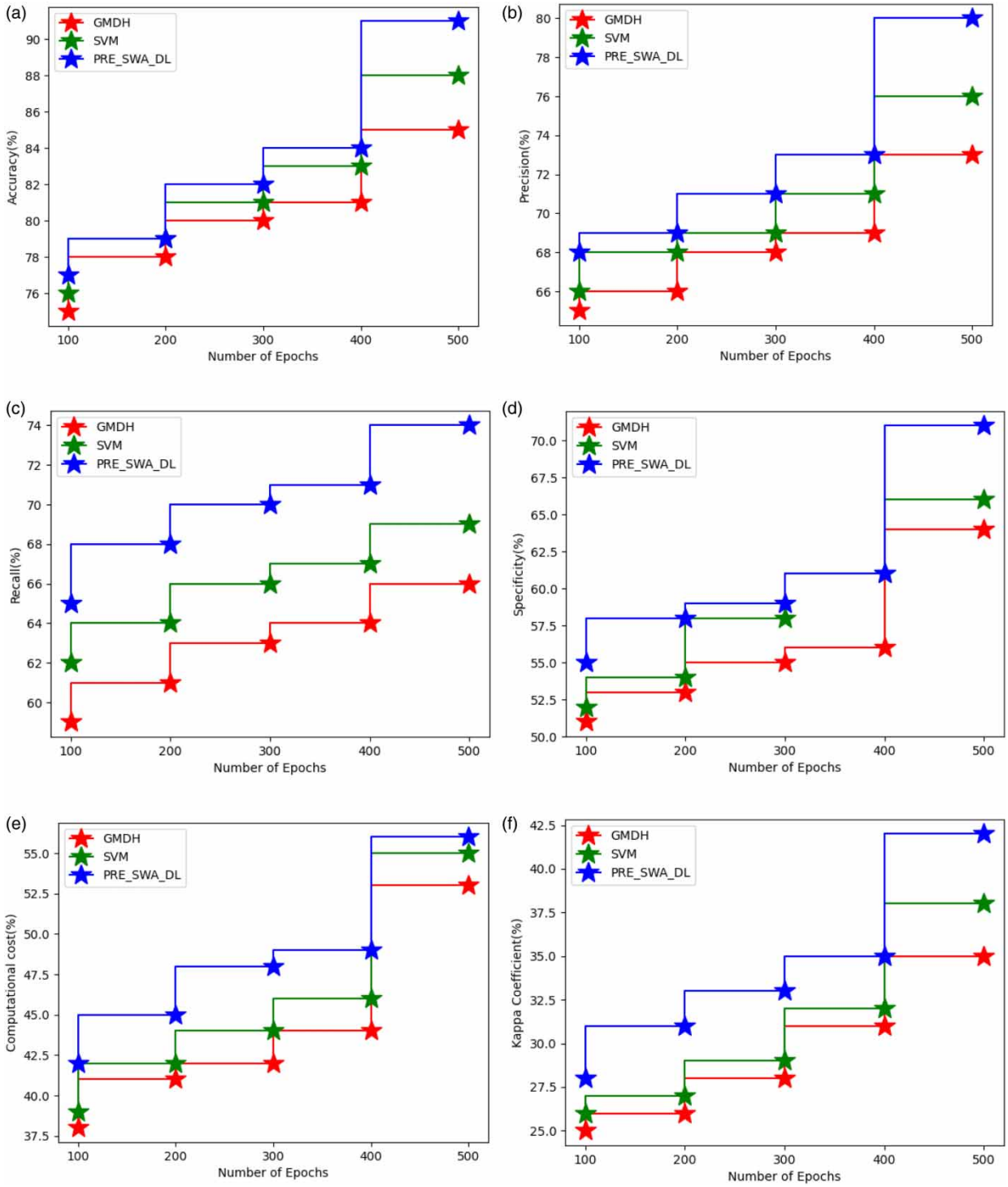

Figure 6 | Comparative analysis between proposed and existing technique for $T_{cond} = 20–30$ °C based on water salinity in terms of (a) Accuracy, (b) Precision, (c) Recall, (d) Specificity, (e) Computational cost, (f) Kappa coefficient.

Figure 7(a)–7(f) gives a comparative analysis between the proposed and existing technique for $T_{evap} = 60–80$ °C based on water salinity. Proposed technique attained accuracy of 96%, precision of 86%, recall of 76%, specificity of 73%, computational cost of 58%, and Kappa coefficient of 45%. The existing GMDH attained accuracy of 93%, precision of 82%, recall

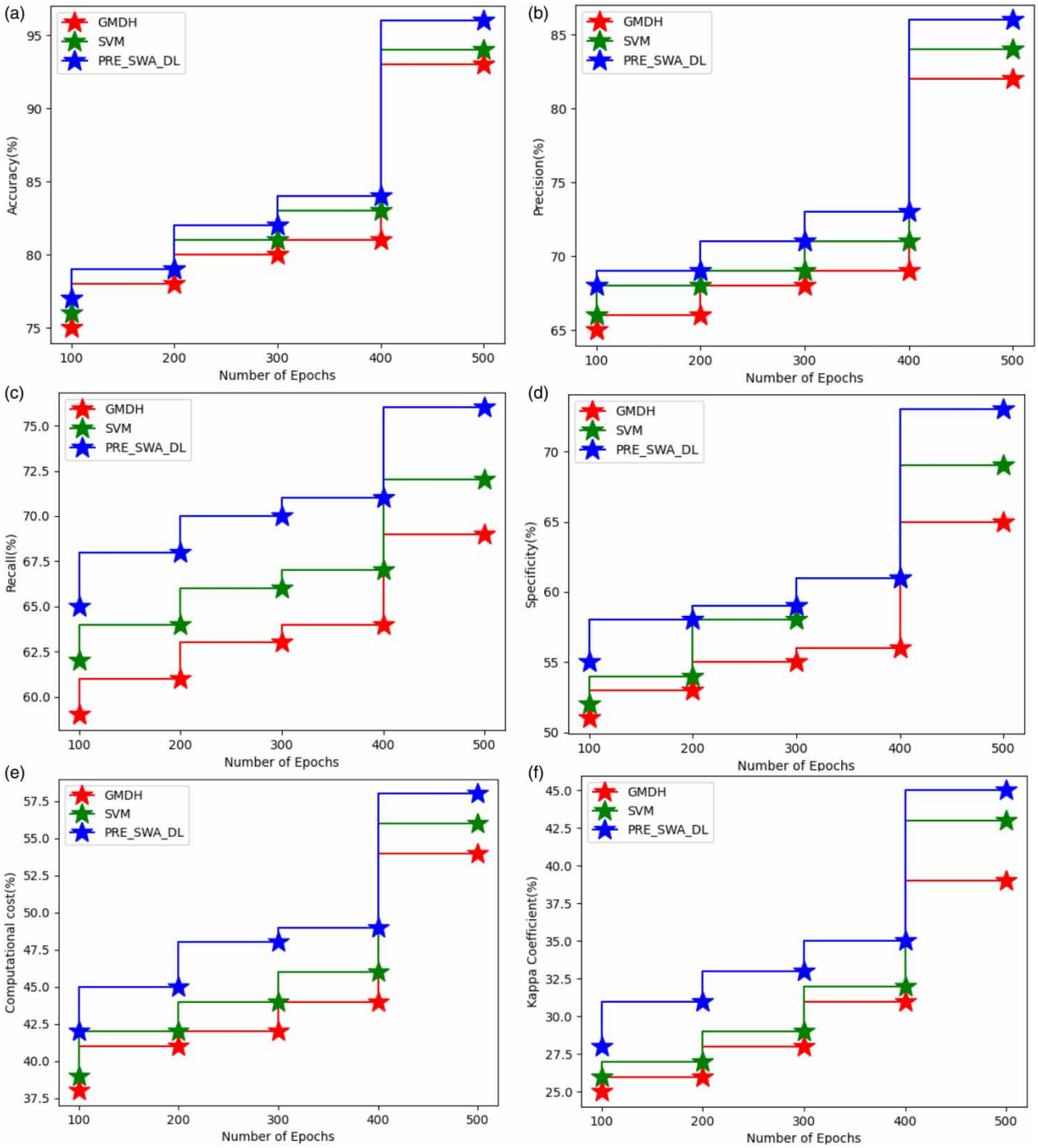

Figure 7 | Comparative analysis between proposed and existing technique for $T_{evap} = 60–80$ °C based on water salinity in terms of (a) Accuracy, (b) Precision, (c) Recall, (d) Specificity, (e) Computational cost, (f) Kappa coefficient.

of 69%, specificity of 65%, computational cost of 54%, and Kappa coefficient of 39%, and SVM attained accuracy of 94%, precision of 84%, recall of 72%, specificity of 69%, computational cost of 56%, and Kappa coefficient of 43%. Hence, deep learning-based models hold great promise for forecasting consumer demands and RES energy generation. However, the efficiency of photovoltaic renewable energy is low compared to other sources of energy. Energy from the sun is intermittent and unpredictable and can only be harnessed in the presence of sunlight.

5. DISCUSSION

Seawater is too salty and has a high concentration of salt ions to be used for drinking or household purposes. Seawater treatment facilities are less effective and dependable. Deep learning systems have the potential to improve efficiency and accuracy of salt particle analysis in saltwater, which will benefit water treatment plant performance. Before implementing the system, the contribution aids manufacturers and research in evaluating the desalination system's productivity in a beta environment. Forecasting energy demand is an essential component of PV that aids in planning of power generation as well as energy trading with commercial grid. Deep learning-based models hold great promise for forecasting consumer demands and RES energy generation.

6. CONCLUSION

This research proposed a novel method in photovoltaic cell in saline water analysis using oxidation process and deep learning techniques based on *Q*-radial function neural networks. Forecasts of renewable availability points are produced using physics-informed ML methods, whose inaccuracy is measured by fitting residuals of the predictor to various statistical distributions using an unsupervised approach. The proposed technique attained accuracy of 96%, precision of 86%, recall of 76%, specificity of 73%, computational cost of 58%, and Kappa coefficient of 45%. In order to more thoroughly analyse the issue of water treatment and create future water treatment systems that are incredibly accurate, we intend to implement our proposed study using hybrid DL methods.

DATA AVAILABILITY STATEMENT

All relevant data are included in the paper or its Supplementary Information.

CONFLICT OF INTEREST

The authors declare there is no conflict.

REFERENCES

Alshehri, M., Kumar, M., Bhardwaj, A., Mishra, S. & Gyani, J. 2021 Deep learning based approach to classify saline particles in sea water. *Water* **13** (9), 1251.

Aslam, S., Herodotou, H., Mohsin, S. M., Javaid, N., Ashraf, N. & Aslam, S. 2021 A survey on deep learning methods for power load and renewable energy forecasting in smart microgrids. *Renewable and Sustainable Energy Reviews* **144**, 110992.

Bu, M., Liang, W., Lu, G. & Yu, J. 2021 Local structure elucidation and properties prediction on KCl–$CaCl_2$ molten salt: a deep potential molecular dynamics study. *Solar Energy Materials and Solar Cells* **232**, 111346.

Coşgun, A., Günay, M. E. & Yıldırım, R. 2021 Exploring the critical factors of algal biomass and lipid production for renewable fuel production by machine learning. *Renewable Energy* **163**, 1299–1317.

Dave, A., Mitchell, J., Kandasamy, K., Wang, H., Burke, S., Paria, B., Póczos, B., Whitacre, J. & Viswanathan, V. 2020 Autonomous discovery of battery electrolytes with robotic experimentation and machine learning. *Cell Reports Physical Science* **1** (12), 100264.

Elsheikh, A. H., Shanmugan, S., Sathyamurthy, R., Thakur, A. K., Issa, M., Panchal, H., Muthuramalingam, T., Kumar, R. & Sharifpur, M. 2022 Low-cost bilayered structure for improving the performance of solar stills: performance/cost analysis and water yield prediction using machine learning. *Sustainable Energy Technologies and Assessments* **49**, 101783.

Hu, G. & You, F. 2022 Renewable energy-powered semi-closed greenhouse for sustainable crop production using model predictive control and machine learning for energy management. *Renewable and Sustainable Energy Reviews* **168**, 112790.

Jamei, M., Karbasi, M., Olumegbon, I. A., Mosharaf-Dehkordi, M., Ahmadianfar, I. & Asadi, A. 2021 Specific heat capacity of molten salt-based nanofluids in solar thermal applications: a paradigm of two modern ensemble machine learning methods. *Journal of Molecular Liquids* **335**, 116434.

Maddah, H. A., Bassyouni, M., Abdel-Aziz, M. H., Zoromba, M. S. & Al-Hossainy, A. F. 2020 Performance estimation of a mini-passive solar still via machine learning. *Renewable Energy* **162**, 489–503.

Meng, F., Zou, Q., Zhang, Z., Wang, B., Ma, H., Abdullah, H. M., Almalaq, A. & Mohamed, M. A. 2021 An intelligent hybrid wavelet-adversarial deep model for accurate prediction of solar power generation. *Energy Reports* **7**, 2155–2164.

Nazari, S., Najafzadeh, M. & Daghigh, R. 2022 Techno-economic estimation of a non-cover box solar still with thermoelectric and antiseptic nanofluid using machine learning models. *Applied Thermal Engineering* **212**, 118584.

Parida, D. R., Dani, N. & Basu, S. 2021 Data-driven analysis of molten-salt nanofluids for specific heat enhancement using unsupervised machine learning methodologies. *Solar Energy* **227**, 447–456.

Pombo, D. V., Bindner, H. W., Spataru, S. V., Sørensen, P. E. & Rygaard, M. 2022 Machine learning-driven energy management of a hybrid nuclear-wind-solar-desalination plant. *Desalination* **537**, 115871.

Said, Z., Sharma, P., Elavarasan, R. M., Tiwari, A. K. & Rathod, M. K. 2022 Exploring the specific heat capacity of water-based hybrid nanofluids for solar energy applications: a comparative evaluation of modern ensemble machine learning techniques. *Journal of Energy Storage* **54**, 105230.

Salem, H., Kabeel, A. E., El-Said, E. M. & Elzeki, O. M. 2022a Predictive modelling for solar power-driven hybrid desalination system using artificial neural network regression with Adam optimization. *Desalination* **522**, 115411.

Salem, H., El-Hasnony, I. M., Kabeel, A. E., El-Said, E. M. & Elzeki, O. M. 2022b Deep learning model and classification explainability of renewable energy-driven membrane desalination system using evaporative cooler. *Alexandria Engineering Journal* **61** (12), 10007–10024.

Shalaby, S. M., Sharshir, S. W., Kabeel, A. E., Kandeal, A. W., Abosheiasha, H. F., Abdelgaied, M., Hamed, M. H. & Yang, N. 2022 Reverse osmosis desalination systems powered by solar energy: preheating techniques and brine disposal challenges – a detailed review. *Energy Conversion and Management* **251**, 114971.

Sharma, P., Said, Z., Kumar, A., Nizetic, S., Pandey, A., Hoang, A. T., Huang, Z., Afzal, A., Li, C., Le, A. T., Nguyen, X. P. & Tran, V. D. 2022 Recent advances in machine learning research for nanofluid-based heat transfer in renewable energy system. *Energy & Fuels* **36** (13), 6626–6658.

Sohani, A., Hoseinzadeh, S., Samiezadeh, S. & Verhaert, I. 2022 Machine learning prediction approach for dynamic performance modeling of an enhanced solar still desalination system. *Journal of Thermal Analysis and Calorimetry* **147** (5), 3919–3930.

Tang, L., Zhou, Y., Zheng, S. & Zhang, G. 2020 Exergy-based optimisation of a phase change materials integrated hybrid renewable system for active cooling applications using supervised machine learning method. *Solar Energy* **195**, 514–526.

Trappey, A. J., Chen, P. P., Trappey, C. V. & Ma, L. 2019 A machine learning approach for solar power technology review and patent evolution analysis. *Applied Sciences* **9** (7), 1478.

Wang, Y., Kandeal, A. W., Swidan, A., Sharshir, S. W., Abdelaziz, G. B., Halim, M. A., Kabeel, A. E. & Yang, N. 2021 Prediction of tubular solar still performance by machine learning integrated with Bayesian optimization algorithm. *Applied Thermal Engineering* **184**, 116233.

Wang, W., Ma, Y., Maroufmashat, A., Zhang, N., Li, J. & Xiao, X. 2022 Optimal design of large-scale solar-aided hydrogen production process via machine learning based optimisation framework. *Applied Energy* **305**, 117751.

First received 24 October 2022; accepted in revised form 15 January 2023. Available online 1 February 2023